Selective and rapid removal of Mo(VI) from water using functionalized Fe_3O_4-based Mo(VI) ion-imprinted polymer

Lang Wu, Zhengwei Luo, Hui Jiang, Zijian Zhao and Wenhua Geng

ABSTRACT

Fe_3O_4 nanoparticles-based magnetic Mo(VI) surface ion-imprinted polymer (Mo(VI)-MIIP) was elaborated employing 4-vinyl pyridine as a functional monomer. The adsorbent preparation was confirmed by Fourier-transform infrared spectroscopy, scanning electron microscopy, energy dispersive X-ray spectrometry, X-ray diffraction, vibrating sample magnetometer, thermogravimetric analysis, and surface area analysis. Batch adsorption experiments showed that the maximum adsorption capacity of Mo(VI)-MIIP was 296.40 mg g^{-1} at pH 3, while that of the magnetic non-imprinted polymer (MNIP) was only 147.10 mg g^{-1}. The adsorption isotherm model was well fitted by the Langmuir isotherm model. The adsorption experiments revealed that Mo(VI)-MIIP reached adsorption equilibrium within 30 min, and the kinetics data fitting showed that the pseudo-second-order kinetics model suitably described the adsorption process. Mo(VI)-MIIP exhibited an excellent adsorption selectivity to Mo(VI) in binary mixtures of Mo(VI)/Cr(VI), Mo(VI)/Cu(II), Mo(VI)/$H_2PO4^-_4$, Mo(VI)/Zn(II), and Mo(VI)/I^-, with relative selectivity coefficients toward MNIP of 13.71, 30.27, 20.01, 23.53, and 15.89, respectively. After six consecutive adsorption-desorption cycles, the adsorption capacity of Mo(VI)-MIIP decreased by 9.5% (from 228.4 mg g^{-1} to 206.7 mg g^{-1} at initial Mo(VI) concentration of 250 mg L^{-1}), demonstrating its reusability.

Key words | ion-imprinted polymers, magnetic nanoparticles, Mo(VI) ions, selective adsorption, surface imprinting

Lang Wu
Zhengwei Luo
Hui Jiang
Zijian Zhao
Wenhua Geng (corresponding author)
College of Biotechnology and Pharmaceutical Engineering,
Nanjing Tech University,
30 # Puzhu South Road, Nanjing 211816,
China
E-mail: *gengwenhua@njtech.edu.cn*

HIGHLIGHTS

- Magnetic surface ion-imprinted polymer was synthesized for rapid and selective removal Mo(VI) from aqueous solution.
- The effects of pH value, contact time and initial concentration on the adsorption process were investigated.
- Mo(VI) adsorption followed the pseudo-second-order kinetics and Langmuir isotherm model.
- Magnetic surface ion-imprinted polymer showed high selectivity for Mo(VI) in the presence of competitive ions.

doi: 10.2166/wst.2020.594

GRAPHICAL ABSTRACT

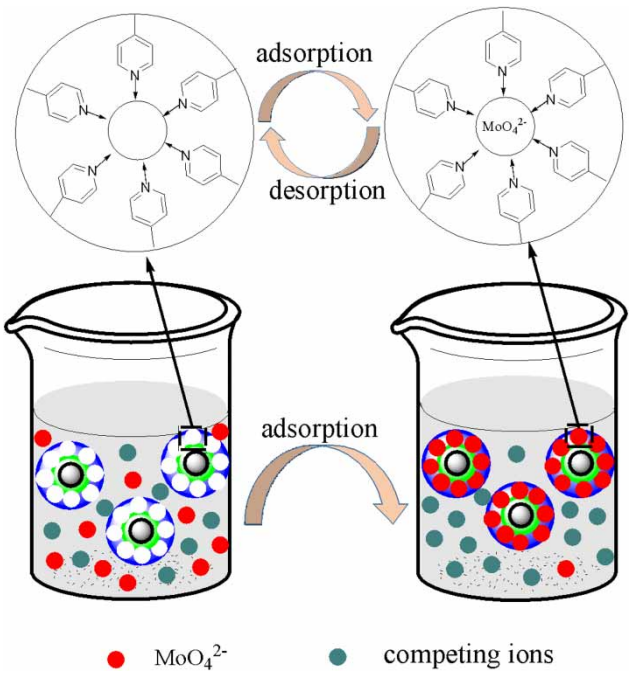

INTRODUCTION

Molybdenum (Mo) is a rare metal with a high melting point, small thermal expansion coefficient, good conductivity and wear resistance, which has been widely used in high-strength steel alloys, thermocouples, electron tubes, and coatings (Xiong *et al.* 2011). Mo forms ions in various oxidation states in the range of −2 to +6, and the oxyanion MoO_4^{2-} is the principal form of soluble Mo in environmental pollution (Du *et al.* 2003). Although Mo is necessary for humans and animals, high concentrations of Mo can cause many diseases such as delayed growth, anemia, bone deformation, liver abnormality, and even death (Atia 2008). Water-soluble Mo(VI) ions at concentrations exceeding 5 mg L^{-1} will lead to environmental pollution, and the permissible Mo concentration should be below 0.07 mg L^{-1} for potable water (Ardau *et al.* 2012). Thus, it is necessary to treat industrial wastewater containing Mo(VI) before discharge.

To date, different methods for removing Mo(VI) ions have been developed, such as constructed wetlands, ion exchange, membrane separation, precipitation, and adsorption (Peng *et al.* 2014; Lou *et al.* 2015). These methods have several shortcomings, such as the generation of non-degradable chemical sludge in chemical precipitation, the low processing efficiency of constructed wetlands, the high energy consumption of membrane separation, and the easy oxidation of the resin in ion-exchange methods. In contrast, adsorption is a practical and economical treatment method with a high efficiency, simple operation, large-scale treatment, environmental friendliness, and low cost. Numerous adsorption materials have been investigated to separate Mo(VI), including alumina, natrolite, activated carbon, chitosan, nano-scale zero-valent iron, and silica gel particles (Fallah *et al.* 2018; He *et al.* 2019). However, these adsorbents suffer from serious drawbacks that must be considered in practical applications, such as poor recyclability, lack of selectivity, and long adsorption time. Thus, there is a need to synthesize adsorbents for Mo(VI) ions with rapid adsorption-desorption kinetics, strong adsorption selectivity, high adsorption capacity, and recyclability. These adsorbents should also be easily and rapidly separated from solution.

Molecular imprinting reversibly immobilizes template molecules on high cross-linked polymers to form molecular imprinting cavities, which produces a memory effect for the size and geometry of the template molecules (Zheng & Yoshikawa 2015). Ion imprinting is a type of molecular

imprinting that corresponds to ion-imprinted polymers (IIP) with imprinting cavities that are complementary to the three-dimensional structure of the template ions (He *et al.* 2018). In general, the preparation of IIP is divided into three steps (Tsoi *et al.* 2012; Najafi *et al.* 2013). First, template ions and functional monomers form coordination compounds through electrostatic interactions or coordination bonds. Then, cross-linkers and initiators are used to polymerize the coordination compounds into polymers. Finally, template ions are eluted from the polymers to produce special ion imprinting sites. Despite having abundant recognition sites and high selectivity, traditional approaches such as bulk polymerization may produce materials with limitations, including irregular shapes, deep burial of imprinting sites in the bulk polymer, heterogeneously distributed binding sites, high crosslinking density, and low mass-transfer rate. These issues can seriously restrict the broader practical applications of IIP (Fayazi *et al.* 2016; Hassanpour *et al.* 2018). Surface ion-imprinting can solve many of these problems by coating an ion-imprinting layer onto a solid support.

With the development of surface imprinting techniques, ion-imprinted materials have been coated on different carriers, including graphene oxide, multi-walled carbon nanotubes, chitosan, SiO_2, ceramic membranes, and Fe_3O_4 nanoparticles (NPs) (Ren *et al.* 2013; Xiong *et al.* 2017; Zeng *et al.* 2017). Fe_3O_4 NPs can be recycled using an external magnetic field rather than complicated separation steps. In addition, magnetic Fe_3O_4 NPs have high mechanical stability, excellent magnetic responsiveness, large specific surface areas, low toxicity, and low cost, making them ideal candidate materials (Dahaghin *et al.* 2017a, 2017b). Therefore, IIP synthesized using Fe_3O_4 NPs as the support should display the advantages of both magnetic nanoparticles and surface ion-imprinted polymers.

Some studies have been conducted on the synthesis IIP for Mo(VI) adsorption (Ren *et al.* 2013; Gao *et al.* 2014; Zhang *et al.* 2014; Hassanpour & Taghizadeh 2016; Zeng *et al.* 2017; Fallah *et al.* 2018); however, there are few reports on the preparation of IIP using Fe_3O_4 NPs as a support and 4-vinyl pyridine (4-VP) as a monomer to selectively adsorb Mo(VI) anions from solution. In this work, a novel IIP was obtained by using 4-VP as a functional monomer, and Fe_3O_4 NPs modified with 3-vinyltriethoxysilane as the support, and the prepared adsorbent was characterized. To determine the Mo(VI) adsorption mechanism, the adsorption kinetics and isotherms were studied. Furthermore, the adsorption capacity, adsorption selectivity, as well as reusability of the fabricated adsorbent were investigated.

EXPERIMENTAL

Materials

Dimethyl sulfoxide (DMSO), 4-vinyl pyridine (4-VP), ethylene glycol methacrylate (EGDMA), *N*, *N*-azobisisobutyronitrile (AIBN), and 3-vinyltriethoxysilane were obtained from Aladdin Industrial Corporation (Shanghai, China). Ferrous chloride tetrahydrate ($FeCl_2{\cdot}4H_2O$), ferric chloride hexahydrate ($FeCl_3{\cdot}6H_2O$), and sodium molybdate dihydrate ($Na_2MoO_4{\cdot}2H_2O$) were obtained from SinSSo-pharm Chemical Reagent Co., Ltd (Shanghai, China). All other chemical reagents used in this work were of reagent grade and purchased from Ocean Chemical Limited Company (Qingdao, China).

Elaboration of the adsorbent

Synthesis of Fe_3O_4 NPs

Fe_3O_4 magnetic nanoparticles were prepared by the chemical co-precipitation of Fe^{2+} and Fe^{3+} ions (Akhond *et al.* 2016; Bukowska *et al.* 2017). Briefly, 4.72 g of $FeCl_3{\cdot}6H_2O$ and 1.72 g of $FeCl_2{\cdot}4H_2O$ were dissolved in 80 mL of deionized water with the inlet of nitrogen gas (N_2). The resulting solution was gradually heated up to 80 °C, and N_2 was continuously aerated to expel oxygen and create an inert condition. Then, after adding 10 mL of ammonia aqueous solution (25%, w/w) dropwise under mechanical stirring, the color of the solution changed from brown to black. The mixture was stirred vigorously under nitrogen gas flow for 30 min to obtain black Fe_3O_4 NPs precipitates. The synthesized Fe_3O_4 NPs were washed with deionized water five times and dried under vacuum at 40 °C.

Functionalization of Fe_3O_4 nanoparticles

Vinyl functionalized Fe_3O_4 nanoparticles (Fe_3O_4@VTES NPs) were prepared using 3-vinyltriethoxysilane to modify the surface of the Fe_3O_4 NPs (Dahaghin *et al.* 2017a, 2017b). Typically, 1.0 g of Fe_3O_4 NPs was dispersed in DMSO (70 mL) under sonication. Afterward, 2.0 mL of 3-vinyltriethoxysilane was added slowly to the solution, and the reaction mixture was stirred for 24 h at room temperature. The resultant black solid was separated, washed, and dried to obtain surface modified Fe_3O_4@VTES NPs.

Preparation of IIP

To prepare Mo(VI)-MIIP, 0.8 g of Fe_3O_4@VTES NPs were homogeneously dispersed in 40 mL of ethanol aqueous solution (60%, v/v) under sonication for 15 min to form suspension (a). Meanwhile, 8 mmol of 4-VP and 0.48 g of $Na_2MoO_4{\cdot}2H_2O$ were dissolved in 80 mL of ethanol aqueous solution (60%, v/v) and stirred for 60 min to form a solution (b). Afterward, solution (b) was mixed with suspension (a) under stirring to form suspension (c). Then, 16 mmol of EGDMA and 80 mg of AIBN were added to the suspension (c). Polymerization was performed at 60 °C for 48 h under nitrogen gas flow to obtain magnetic surface ion-imprinted polymers containing Mo(VI) ions. Subsequently, the resultant polymers were separated and washed to remove unreacted monomers and other impurities. Mo(VI) ions were eluted from ion-imprinted polymers with 0.05 M NaOH for 45 min. This was repeated until Mo(VI) ions were not detected in the elution solution using ICP-OES. Finally, the obtained Mo(VI)-MIIP was washed with deionized water and dried in a vacuum oven for 12 h at 60 °C. In contrast, magnetic non-imprinted polymers (MNIP) were simultaneously synthesized using the same procedure, except the template ion was omitted. Figure 1 illustrates the preparation procedure of Mo(VI)-MIIP.

Characterization

The functional groups were identified by Fourier transform infrared spectroscopy (FT-IR, Nicolet 6700, Thermo Fisher, USA). XRD patterns were obtained using an X-ray diffractometer (XRD, Bruker D8 Advance, Germany). Scanning electron microscopy (SEM, Thermo Fisher, USA) and energy dispersive spectroscopy (EDS) were used to evaluate the surface morphology and elementary analysis. Thermogravimetric analysis (TGA) was studied using a Perkin Elmer TGA 400 (New Castle, USA). The magnetic property was analyzed using a vibrating sample magnetometer (VSM, VersaLab, USA). The Brunauer-Emmett-Teller (BET) surface area and average pore sizes were obtained from nitrogen adsorption/desorption experiments using a

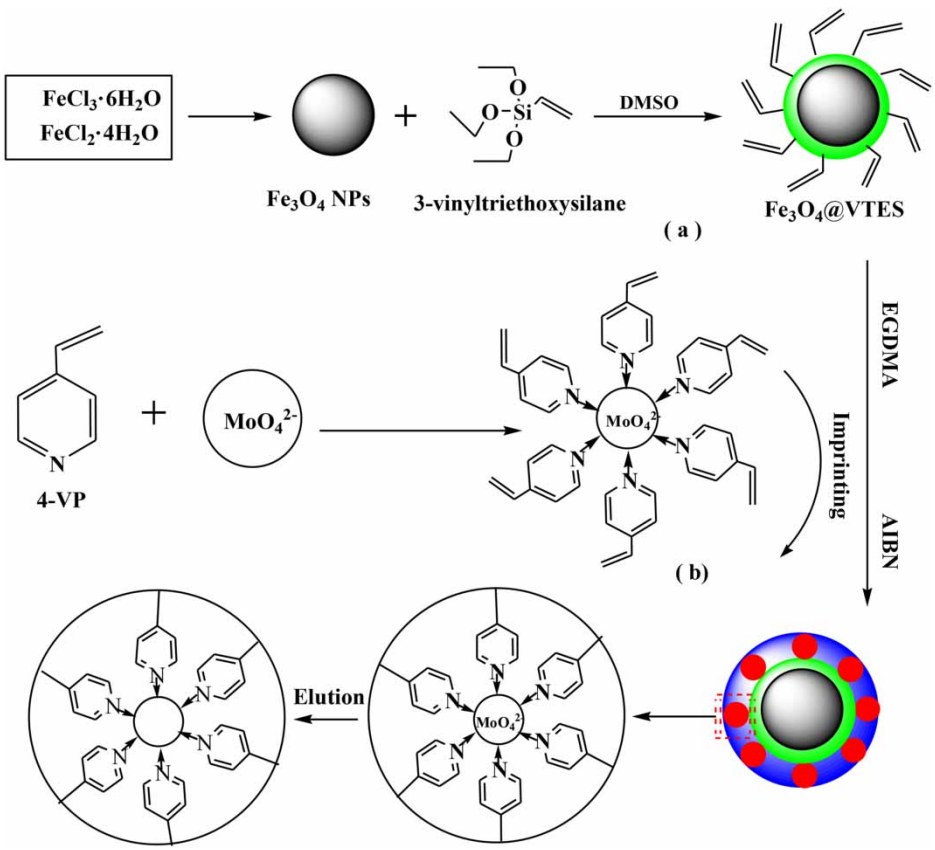

Figure 1 | The schematic diagram for the synthesis of Mo(VI)-MIIP.

V-Sorb 2800 Series Analyzer (Gold APP Instrument, Beijing, China).

Adsorption experiments

Adsorption experiments were performed in glass serum bottles, each containing 10 mL of Mo(VI) ions solution and 10 mg of the adsorbent. Then, the bottles were shaken at 200 rpm. Afterward, the adsorbent was separated by an external magnetic field, and the residual concentration of Mo(VI) ions was determined by inductively coupled plasma-optical emission spectrometer (ICP-OES, iCAP 6300, Thermo Fisher, USA). The adsorption capacity q_e (mg g^{-1}) was calculated using Equation (1):

$$q_e = \frac{(c_i - c_e)V}{m} \quad (1)$$

where c_i (mg L^{-1}) and c_e (mg L^{-1}) are the initial and equilibrium concentrations of Mo(VI) ions, respectively; V (L) is the volume of the solution; and m (g) is the mass of Mo(VI)-MIIP or MNIP.

Adsorption selectivity

The adsorption selectivity of Mo(VI)-MIIP to Mo(VI) ions was studied in the presence of Cu(II), Cr(VI), Zn(II), $H_2PO4^-_4$, and I^- as competing ions in binary mixtures. The concentrations of Mo(VI) and competing ions were both 250 mg L^{-1} in the solution. After a certain period of time, the adsorbent was separated and the concentrations of Mo(VI) and competing ions were determined by ICP-OES. The distribution coefficient (K_d [L g^{-1}]) and selectivity coefficient (K) of Mo(VI) for competing ions were calculated using Equations (2) and (3). The relative selectivity coefficient (K') was calculated using Equation (4):

$$K_d = \frac{q_e}{c_e} \quad (2)$$

$$K = \frac{K_d(\text{template})}{K_d(\text{competing})} \quad (3)$$

$$K' = \frac{K_{IIP}}{K_{NIP}} \quad (4)$$

RESULTS AND DISCUSSION

Characterization

FT-IR

The FT-IR spectra of Fe_3O_4, Fe_3O_4@VTES, and Mo(VI)-MIIP are shown in Figure 2. For Fe_3O_4 (curve (a)), the peak of -OH stretching vibration at 3,425 cm^{-1} was probably attributed to the hydroxyl groups on the surface of Fe_3O_4 or the residual water in the sample (Li *et al.* 2016). The stretching vibration of the Fe-O bond in Fe_3O_4 at 568 cm^{-1} moved to the vicinity of 534 cm^{-1} after coating with silane coupling agent (curve (b)) and ion-imprinted layer (curve (c)), which indicated the successful synthesis of Fe_3O_4 NPs (Qi *et al.* 2017; Zhou *et al.* 2020). In curve (b), the peaks located at 764 cm^{-1} and 832 cm^{-1} were ascribed to the vibration of Si-O, the peak at 1,097 cm^{-1} was due to the Si-O-Si bond stretching vibration, and the peak at 1,430 cm^{-1} was attributed to the C = C bond asymmetric vibration (Wang *et al.* 2020). These peaks demonstrated that Fe_3O_4 NPs were successfully modified by 3-vinyltriethoxysilane (Hassanpour *et al.* 2018). In curve (c), the C = O absorption peak was observed at 1,665 cm^{-1}, and the band near 2,952 cm^{-1} was due to the C-H stretching vibration, which were originated from the crosslinker EGDMA (Li *et al.* 2018). Meanwhile, the C = N asymmetric vibration peak at 1,725 cm^{-1} was due to the pyridine ring of 4-VP (Ren *et al.* 2013; Liang *et al.* 2017). These results verified the fabrication of Mo(VI)-MIIP.

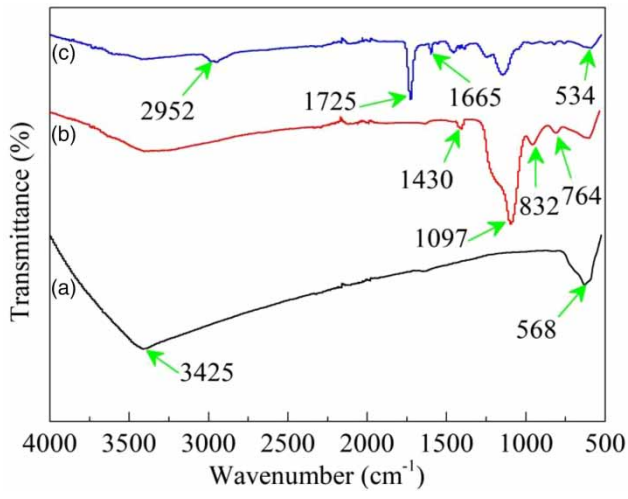

Figure 2 | FT-IR spectra of (a) Fe_3O_4, (b) Fe_3O_4@VTES, and (c) Mo(VI)-MIIP.

SEM and EDS

The morphology and size of unleached and leached Mo(VI)-MIIP are shown in Figure 3. As can be seen from the SEM micrograph of unleached Mo(VI)-MIIP (Figure 3(a)), the beads of Mo(VI)-MIIP were rough and uneven because of the ion-imprinted layer coated on the surface of the magnetic nanoparticles. In addition, the SEM micrograph also showed that the particles were not isolated but connected to each other due to agglomeration (Elwakeel *et al.* 2020; René *et al.* 2020). After eluting the molybdenum ion with 0.05 M NaOH (Figure 3(b)), the morphology and size of Mo(VI)-MIIP did not significantly change. EDS analysis of Mo(VI)-MIIP before and after elution was carried out, and the obtained elemental spectral analyses are given. As shown in Figure 3(c), C, N, O, Fe, Si, and Mo were the main elements present in Mo(VI)-MIIP before elution. The presence of Fe in Mo(VI)-MIIP indicated that Fe_3O_4 NPs were doped into the polymer matrix (Adauto *et al.* 2020). And the existence of N illustrated the existence of 4-VP as a functional monomer through polymerization reaction (Kumar *et al.* 2019; Yang *et al.* 2020). A comparison of the EDS spectra of Mo(VI)-MIIP before and after elution demonstrated that elution completely removed the template Mo(VI) ions.

XRD

The XRD characterization results of Fe_3O_4, Fe_3O_4@VTES, and Mo(VI)-MIIP are presented in Figure 4. The 2θ peaks

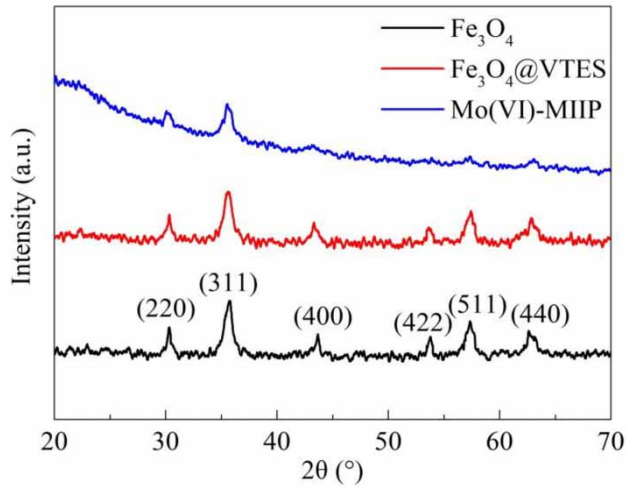

Figure 4 | XRD patterns of Fe_3O_4, Fe_3O_4@VTES, and Mo(VI)-MIIP.

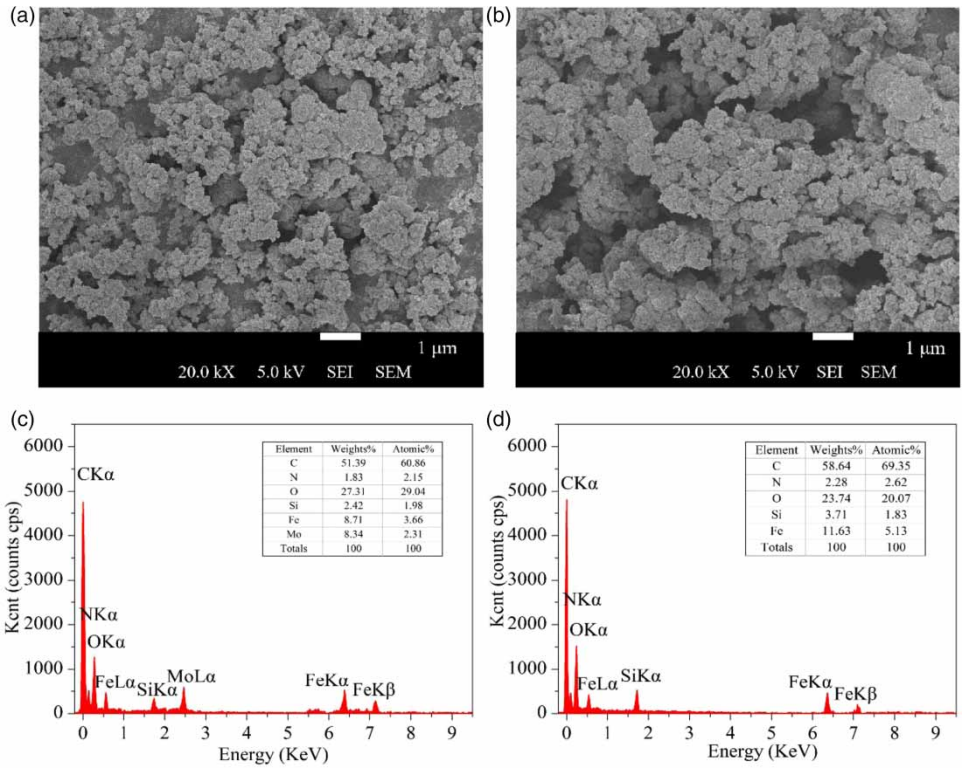

Figure 3 | SEM micrographs of Mo(VI)-MIIP (a) before and (b) after elution, and EDS spectra of Mo(VI)-MIIP (c) before and (d) after elution.

of the synthesized nanoparticles appeared at 29.2°, 35.5°, 43.2°, 53.6°, 57.0°, and 62.7°, indicating a crystalline cubic spinel structure of Fe_3O_4 particles (Tanjim *et al.* 2018). These diffraction peaks of the synthesized nanoparticles matched well with the standard pattern of Fe_3O_4 NPs reported in the JCPDS-International Centre, which demonstrated the successful preparation of Fe_3O_4 NPs (Liang *et al.* 2017). After modification with 3-vinyltriethoxysilane, the diffraction peaks of Fe_3O_4@VTES were nearly unchanged compared with that of Fe_3O_4 NPs. In the XRD spectrum of Mo(VI)-MIIP, the attenuated characteristic diffraction peaks at $2\theta = 29.2°$ and 35.5° were still observed, but the intensity of the peaks at 43.2°, 53.6°, 57.0°, and 62.7° decreased. The reduced diffraction peak intensity was because the ion-imprinted polymers coated the surface of the Fe_3O_4 NPs and attenuated the incident X-rays (Dahaghin *et al.* 2017a, 2017b); however, the diffraction peak positions did not change during adsorbent fabrication. The result indicated that the crystal structure of the Fe_3O_4 NPs was maintained during the polymerization (Shafizadeh *et al.* 2019), which implied that the Fe_3O_4 NPs were encapsulated in Mo(VI)-MIIP.

VSM

The magnetic properties of Fe_3O_4@VTES and Mo(VI)-MIIP were evaluated. According to Figure 5, the hysteresis loops of Fe_3O_4@VTES and Mo(VI)-MIIP were all classic 'S'-shaped curves passing through the origin, which suggested that they had little hysteresis, coercive force, and remnant magnetization (Azizi *et al.* 2017). The results demonstrated that Fe_3O_4@VTES and Mo(VI)-MIIP were superparamagnetic. The saturation magnetization of Fe_3O_4@VTES was measured to be 26.4 emu/g, and the saturation magnetization of Mo(VI)-MIIP decreased to 4.95 emu/g, which was due to the ion-imprinted layer polymerized on Fe_3O_4@VTES. Although the saturation magnetization of Mo(VI)-MIIP decreased after surface imprinting, it could still be rapidly separated from aqueous solution in 15 seconds using an external magnetic field (inserted photograph in Figure 5).

TGA

The thermogravimetric curves of Fe_3O_4, Fe_3O_4@VTES, and Mo(VI)-MIIP are given in Figure 6. The 0.8% decrease in the Fe_3O_4 curve was ascribed to the evaporation of residual water. The TGA curve of Fe_3O_4@VTES was not very different from that of Fe_3O_4, but its slope was steeper than that of Fe_3O_4 because of the decomposition of the silane coupling agent coated on the Fe_3O_4@VTES surface. The residual mass fraction was 91.3%. The weight loss of Mo(VI)-MIIP was divided into three main stages. The first stage occurred from room temperature to 150 °C due to the evaporation of the moisture and residual reagents in Mo(VI)-MIIP particles. The second stage occurred from 150 °C to 500 °C. The adsorbent mass was relatively stable below 300 °C, and the weight loss was only 10.8%; however, the weight of Mo(VI)-MIIP sharply decreased from 300 °C to 500 °C, because of the decomposition and volatilization of organic compounds on the Mo(VI)-MIIP surface. The final stage occurred from 500 °C to 600 °C, during which the weight of the adsorbent

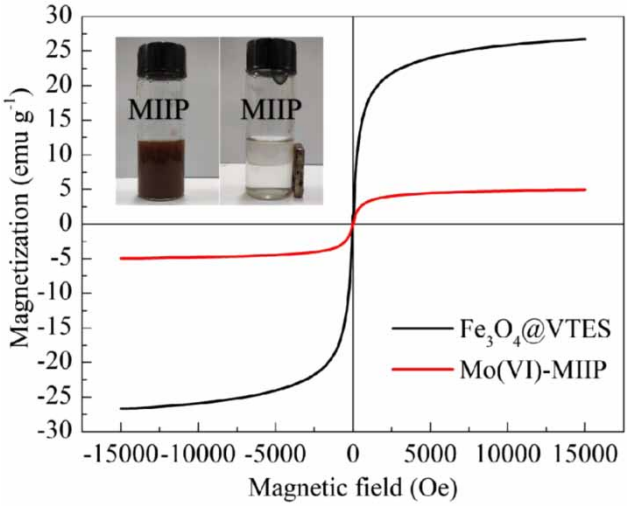

Figure 5 | The VSM spectra of Fe_3O_4@VTES and Mo(VI)-MIIP, and the separation of Mo(VI)-MIIP using a magnet.

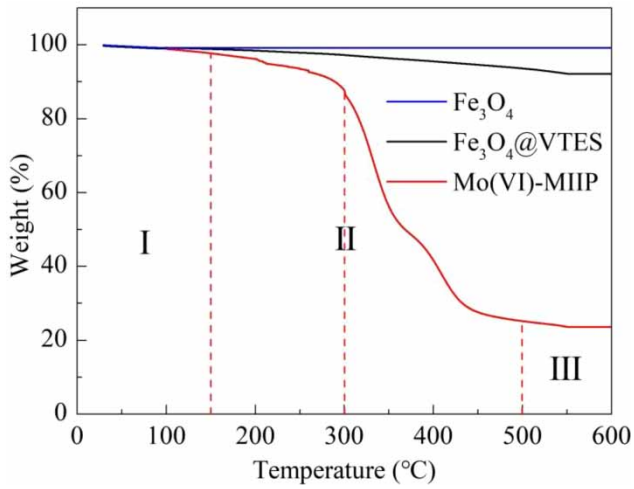

Figure 6 | The weight loss curves of Fe_3O_4, Fe_3O_4@VTES, and Mo(VI)-MIIP.

hardly changed, indicating that the imprinted polymers on the Mo(VI)-MIIP surface had completely decomposed.

Surface area analysis

In the N_2 adsorption-desorption isotherms of Fe_3O_4@VTES and Mo(VI)-MIIP in Figure 7, both adsorption isotherms were typical type IV isotherms (Akbarnejad *et al.* 2019; Hassan *et al.* 2020). The pore size and total pore volume of Fe_3O_4@VTES and Mo(VI)-MIIP were determined by the Barrett-Joyner-Halenda method (Table 1). Fe_3O_4@VTES and Mo(VI)-MIIP had pore sizes of 10.86 nm and 10.23 nm, whereas their total pore volumes were 0.3171 $cm^3\ g^{-1}$ and 0.1156 $cm^3\ g^{-1}$, respectively. In addition, the specific surface areas of Fe_3O_4@VTES and Mo(VI)-MIIP were 88.15 $m^2\ g^{-1}$ and 43.96 $m^2\ g^{-1}$, respectively. The data showed that the synthesized adsorbent was a mesoporous material suitable for binding ions.

Table 1 | Physical properties of Fe_3O_4@VTES and Mo(VI)-MIIP

Samples	Average pore diameter (nm)	Total pore volume ($cm^3\ g^{-1}$)	Specific surface area ($m^2\ g^{-1}$)
Fe_3O_4@VTES	10.86	0.3171	88.15
Mo(VI)-MIIP	10.23	0.1156	43.96

Study of adsorption process

Effect of pH

Solution pH may influence adsorption by changing the valence state of Mo ions and the extent of protonation of N atoms in the functional groups of Mo(VI)-MIIP (Zhang *et al.* 2014). The adsorption of Mo(VI) ions on Mo(VI)-MIIP and MNIP under different pH (2–8) were investigated because oxyanion MoO_4^{2-} is the main ion species of Mo(VI) at the pH range from 3 to 7 in aqueous solution (Ren *et al.* 2013). As illustrated in Figure 8, Mo(VI)-MIIP and MNIP showed the same adsorption capacity variation with the change of solution pH. The maximum Mo(VI) adsorption capacity was reached at pH 3, which showed that the extent of protonation of the N atoms was relatively high, resulting in strong electrostatic interactions between functional groups and oxyanion MoO_4^{2-}. The decreased Mo(VI) adsorption capacity at pH values below 3 was possibly due to the intense competition between positively-charged H^+ ions and Mo(VI) ions (Fallah *et al.* 2018); when the solution pH was between 3 and 4, the adsorption capacity decreased slightly because fewer N atoms were protonated. As the pH increased, the Mo(VI) adsorption capacity was severely reduced because of electrostatic repulsion between the negatively-charged functional groups of adsorbents and oxyanion

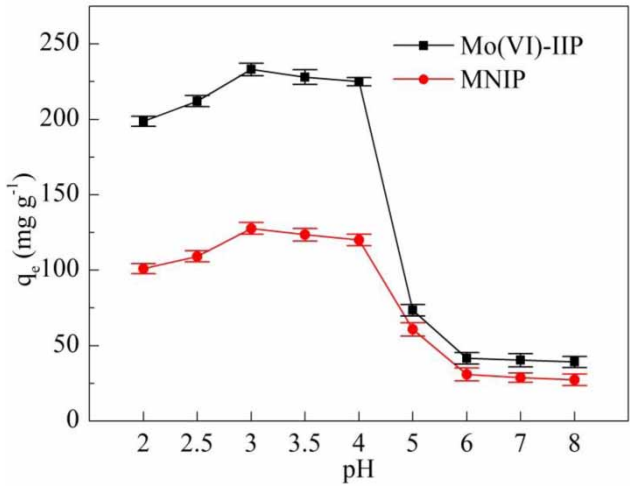

Figure 8 | Effect of pH on Mo(VI) adsorption onto adsorbents (10 mL of Mo(VI) solution (250 mg L^{-1}); 10 mg of adsorbent; 120 min of contact time; 25 ± 2 °C).

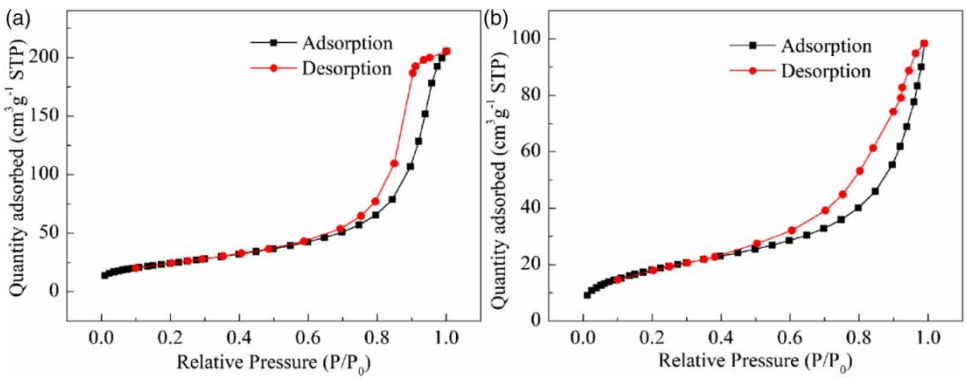

Figure 7 | N_2 adsorption-desorption isotherms of (a) Fe_3O_4@VTES and (b) Mo(VI)-MIIP.

MoO_4^{2-} (Wang *et al.* 2010). Therefore, pH = 3 was the optimal pH in subsequent adsorption experiments.

Adsorption kinetics

The Mo(VI) adsorption capacity of Mo(VI)-MIIP and MNIP over time were investigated. As depicted in Figure 9(a), the amount of Mo(VI) adsorbed onto Mo(VI)-MIIP and MNIP increased rapidly in the first 3 min, and then the adsorbed amount increased slowly until adsorption saturation was reached at 30 min. During the initial stage of adsorption, the relatively fast adsorption rate was attributed to abundant binding sites and the small diffusion resistance of the thin ion-imprinted polymer layer. Upon increasing the adsorption time, the binding sites on the adsorbent surface were gradually consumed, which decreased the adsorption rate until adsorption equilibrium was reached. The amount of Mo(VI) adsorbed by Mo(VI)-MIIP was much higher than MNIP, indicating that Mo(VI)-MIIP possessed a stronger binding affinity for Mo(VI) than MNIP.

Pseudo-first-order kinetics (Equation (5)) and pseudo-second-order kinetics models (Equation (6)) were used to fit the adsorption data.

$$q_t = q_e(1 - e^{-k_1 t}) \tag{5}$$

$$q_t = \frac{k_2 q_e^2}{1 + k_2 q_e t} t \tag{6}$$

where k_1 (min^{-1}) and k_2 ($g\,mg^{-1}\,min^{-1}$) are the pseudo-first-order and pseudo-second-order kinetic rate constants, respectively; q_t ($mg\,g^{-1}$) and q_e ($mg\,g^{-1}$) are the adsorption amount of Mo(VI) at time t and equilibrium, respectively.

The kinetics models for the adsorption of Mo(VI) onto Mo(VI)-MIIP and MNIP are shown in Figure 9(b), and the relevant kinetics fitting parameters are listed in Table 2. The R^2 of the pseudo-second-order kinetics model was closer to 1 than that of the pseudo-first-order kinetics model, and the theoretical adsorption capacity calculated by the pseudo-second-order kinetics model was also closer to the experimental value. The results demonstrated that the pseudo-second-order kinetics model better described Mo(VI) adsorption, indicating that adsorption proceeded via chemical adsorption.

Adsorption isotherms

Equilibrium adsorption isotherm experiments were carried out at initial concentrations from 50 to 700 mg L^{-1}. As illustrated from Figure 10(a), the Mo(VI) adsorption capacity of Mo(VI)-MIIP and MNIP significantly increased upon increasing the initial concentration, and then the adsorption capacity slowly increased before stabilizing. when the initial concentration increased to 400 mg L^{-1}, the adsorption capacity of Mo(VI)-MIIP and MNIP reached adsorption saturation at 296.40 mg g^{-1} and 147.10 mg g^{-1}, respectively.

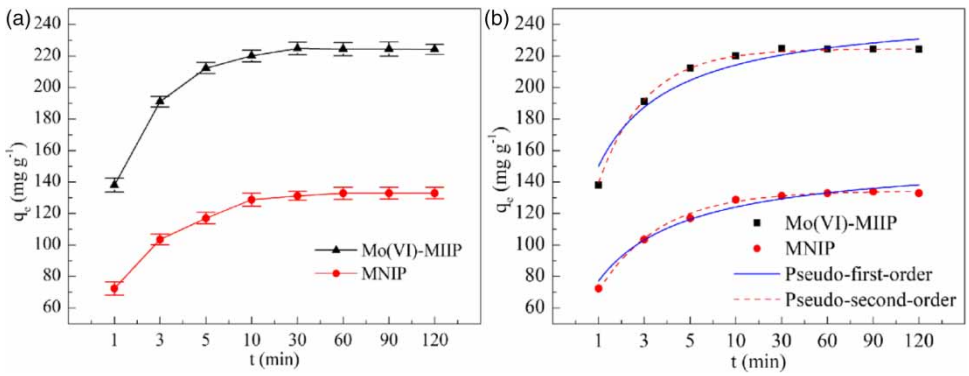

Figure 9 | (a) Kinetics data and (b) fitting of Mo(VI) adsorption by Mo(VI)-MIIP and MNIP (10 mL of Mo(VI) solution (250 mg L^{-1}); 10 mg of adsorbent; pH = 3; 25 ± 2 °C).

Table 2 | Fitting parameters of kinetic models for Mo(VI) adsorption

		Pseudo-first-order			Pseudo-second-order			
Adsorbents	$q_{e,\,exp}$ ($mg\,g^{-1}$)	k_1 (min^{-1})	q_e ($mg\,g^{-1}$)	R^2	k_2 ($g\,mg^{-1}\,min^{-1}$)	q_e ($mg\,g^{-1}$)	h_0	R^2
Mo(VI)-MIIP	224.81	0.0527	249.42	0.912	0.0060	236.55	4.42	0.992
MNIP	133.05	0.0286	155.76	0.958	0.0063	143.49	4.32	0.989

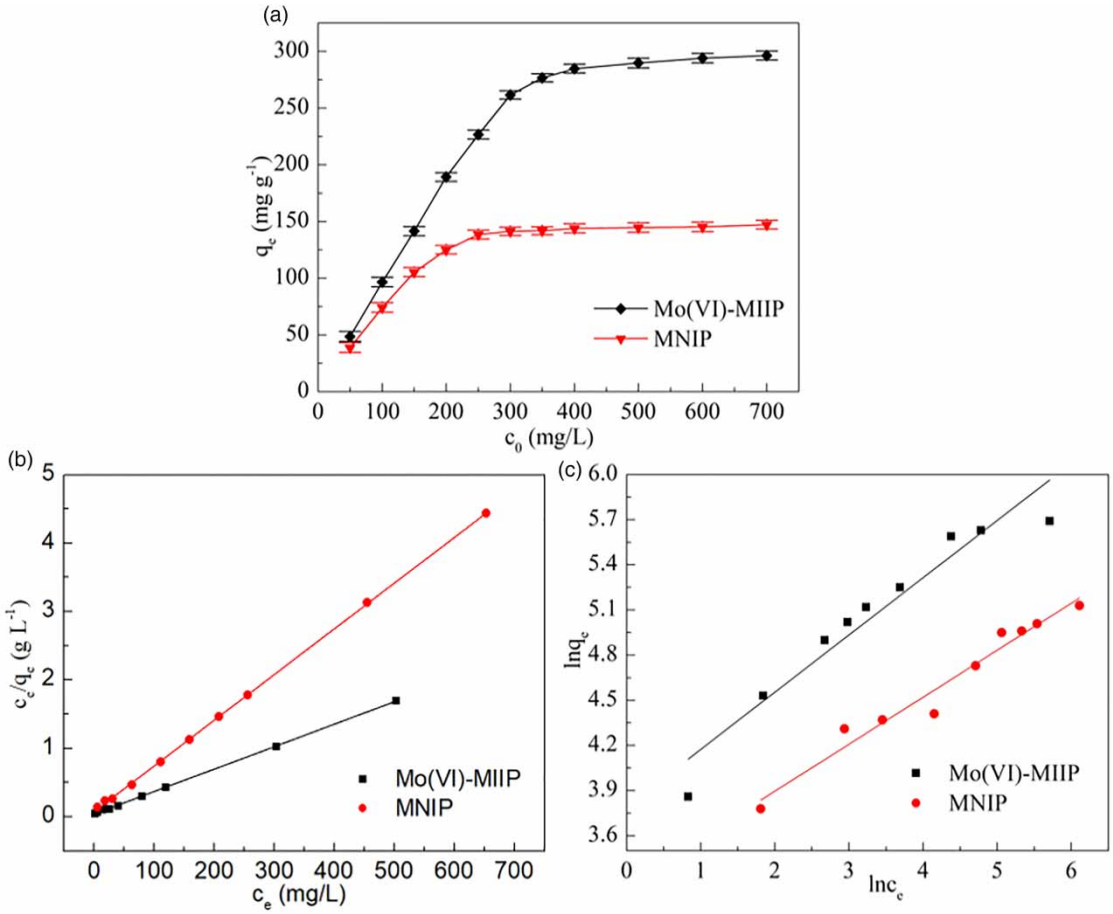

Figure 10 | (a) Adsorption isotherms, (b) Langmuir, and (c) Freundlich fittings of Mo(VI) adsorption onto Mo(VI)-MIIP and MNIP (10 mL of Mo(VI) solution; 10 mg of adsorbent; pH = 3; 30 min of contact time; 25 ± 2 °C).

The adsorption capacity of Mo(VI)-MIIP was 2.01 times higher than MNIP, because of the abundant specific imprinting sites on the Mo(VI)-MIIP surface.

To analyze the relationship between the remaining ions in solution and the amount of ions adsorbed onto Mo(VI)-MIIP and MNIP, Langmuir isotherm (Equation (7)) and Freundlich isotherm (Equation (8)) models were used to fit the experimental data. Usually, the Langmuir isotherm model explains monolayer adsorption on a homogeneous surface and is controlled by chemisorption, while the Freundlich isotherm model describes multilayer adsorption on heterogeneous surface with different types of adsorption sites and is controlled by physisorption (Al Abri *et al.* 2019).

$$\frac{c_e}{q_e} = \frac{c_e}{q_m} + \frac{1}{K_L q_m} \tag{7}$$

$$\ln q_e = \ln K_F + \frac{1}{n} \ln c_e \tag{8}$$

where c_e (mg L^{-1}) is the Mo(VI) ion concentration in solution at adsorption equilibrium; q_e (mg g^{-1}) is the adsorption capacity of Mo(VI) by adsorbents at adsorption equilibrium; q_m (mg g^{-1}) is the theoretical maximum adsorption capacity; K_L (L mg^{-1}) is the Langmuir isotherm model constant; K_F (mg g^{-1}) is the Freundlich isotherm model constant; n represents the Freundlich isotherm model binding constant.

The linear fitting Langmuir isotherm model and Freundlich isotherm model of Mo(VI) adsorbed by Mo(VI)-MIIP and MNIP are described in Figure 10(b) and 10(c), respectively. The relevant isotherm model parameters calculated using Equations (7) and (8) are listed in Table 3. According to Table 3, the correlation coefficients of the Langmuir isotherm model fitted to Mo(VI)-MIIP and MNIP were 0.999 and 0.997, respectively, while the correlation coefficients of the Freundlich isotherm model were 0.932 and 0.958, respectively. The correlation coefficients indicated that Mo(VI) adsorption was better described by the Langmuir isotherm model, demonstrating that the adsorption of

Table 3 | Langmuir and Freundlich isotherm model parameters for Mo(VI) adsorption onto Mo(VI)-MIIP and MNIP

	Langmuir			Freundlich		
Adsorbents	q_m (mg g^{-1})	K_L (L mg^{-1})	R^2	n	K_F (mg g^{-1})	R^2
Mo(VI)-MIIP	304.87	0.084	0.999	2.63	43.31	0.923
MNIP	149.70	0.091	0.997	3.23	22.68	0.958

Mo(VI) ions onto Mo(VI)-MIIP and MNIP occurred via monolayer chemisorption, and the result corresponded with the pseudo-second-order kinetics model. The theoretical maximum absorption capacities of Mo(VI)-MIIP and MNIP obtained from the Langmuir isotherm model curve were 304.87 mg g^{-1} and 149.70 mg g^{-1}, respectively, which were very similar to the experimental values (296.40 mg g^{-1} and 147.10 mg g^{-1}, respectively). The comparison of Mo(VI)-MIIP with other adsorbents reported in the literatures is listed in Table 4. It can be concluded that the prepared Mo(VI)-MIIP showed a considerably higher adsorption capacity and short equilibrium time.

Adsorption selectivity

The adsorption selectivity of Mo(VI)-MIIP was studied in the presence of competing ions in binary mixtures. Cr(VI), Cu(II), $H_2PO4_4^-$, Zn(II), and I^- were chosen as latent competing ions because of their similar properties to Mo(VI) or their common occurrence in wastewater. Table 5 displays

Table 4 | Comparison of adsorption performances of different adsorbents for Mo(VI)

Adsorbents	**Capacity (mg g^{-1})**	**Equilibrium time (min)**	**References**
SiO_2-IIP	208.60	75	Ren *et al.* (2013)
IIP-DMAEMA	45.20	90	Gao *et al.* (2014)
IIP-CTS/TEA	351.40	500	Zhang *et al.* (2014)
IIP-SCN	3.77	20	Ardestani *et al.* (2016)
IIP-MAA	31.10	30	Hassanpour & Taghizadeh (2016)
PVI/CM-IIP	64.80	540	Zeng *et al.* (2017)
IIP-4-PA	126.10	10	Fallah *et al.* (2018)
Fe_3O_4-MIIP	296.40	30	This work

Table 5 | Distribution coefficient, selectivity coefficient and relative selectivity coefficient for Mo(VI)-MIIP and MNIP

Ions	Mo(VI)-MIIP			MNIP			
	q (mg g^{-1})	K_d	K	q (mg g^{-1})	K_d	K	K'
Mo(VI)	202.92	4.31	15.35	66.72	0.37	1.12	13.71
Cr(VI)	53.60	0.28		62.73	0.33		
Mo(VI)	219.59	7.22	48.13	74.42	0.43	1.59	30.27
Cu(II)	31.40	0.15		53.61	0.27		
Mo(VI)	210.57	5.34	23.21	72.88	0.42	1.16	20.01
$H_2PO4_4^-$	46.52	0.23		66.32	0.36		
Mo(VI)	218.03	5.95	37.18	72.13	0.41	1.58	23.53
Zn(II)	35.81	0.16		51.80	0.26		
Mo(VI)	206.37	4.73	18.92	68.32	0.38	1.19	15.89
I^-	49.07	0.25		60.54	0.32		

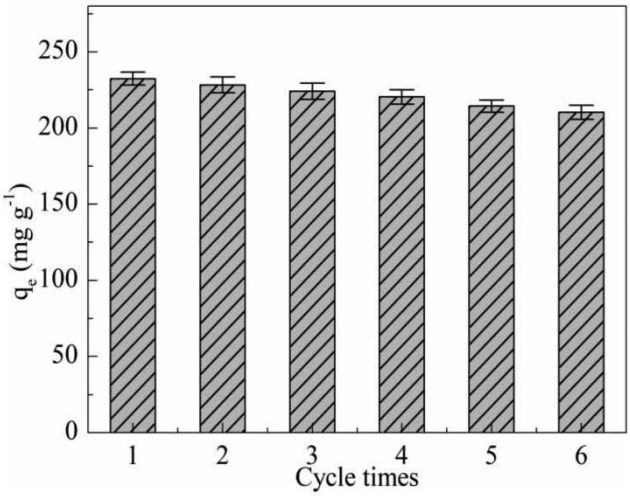

Figure 11 | Reusability of Mo(VI)-MIIP for Mo(VI) removal (10 mL of Mo(VI) solution (250 mg L^{-1}); 10 mg of adsorbent; pH = 3; 30 min of contact time; 25 ± 2 °C).

K_d, K, and K' toward competing ions by Mo(VI)-MIIP and MNIP. The adsorption amount of Mo(VI)-MIIP to Mo(VI) was more than four times higher than competing ions, because there were many special imprinting cavities on Mo(VI)-MIIP that matched the size and geometry of Mo(VI). However, under the same competitive adsorption conditions, the adsorption amount of MNIP to Mo(VI) was similar to competing ions (Mercante *et al.* 2020). These results also showed that anions had a more significant influence on Mo(VI) adsorption by Mo(VI)-MIIP because the competitive anions also combined with positively-charged functional groups on the adsorbents (Kong *et al.* 2014). Despite this, the K' values (Table 5) showed that Mo(VI)-MIIP had a strong adsorption selectivity to Mo(VI) compared with MNIP.

Reusability

The reusability of synthesized adsorbents are important for their industrial applications. Six adsorption-desorption cycles were performed to study the reusability of magnetic Mo(VI)-MIIP, and 0.05 M NaOH solution was used as the eluent. As given in Figure 11, the adsorption capacity of Mo(VI)-MIIP decreased from 228.40 mg g^{-1} to 206.70 mg g^{-1} after six adsorption-desorption cycles, retaining 90.5% of its initial adsorption. The slight decrease in adsorption capacity of Mo(VI)-MIIP was mainly because of partial damage to the imprinting recognition sites on the surface of the adsorbent after repeated elution (Nchoe *et al.* 2020). Nevertheless, the difference in adsorption capacity was not significant after six cycles, revealing that Mo(VI)-MIIP possessed a favorable stability and regeneration ability.

CONCLUSIONS

A novel Mo(VI)-MIIP capable of surface ion-imprinting, magnetic separation, and intelligent adsorption was synthesized and used to selectively and rapidly separate Mo(VI) from aqueous solution. The morphological characteristics and compositions of the fabricated Mo(VI)-MIIP were analyzed by various techniques. The obtained magnetic Mo(VI)-MIIP exhibited a prominent adsorption performance for Mo(VI) (296.20 mg g^{-1}) and a short adsorption equilibrium time (30 min) at pH 3. It also showed an outstanding selectivity for Mo(VI) in the existence of both interfering anions and cations, because of the abundant and unique imprinting cavities on the surface of Mo(VI)-MIIP. The Langmuir isotherm model and pseudo-second-order kinetics model fittings of the experiment data demonstrated that Mo(VI) adsorption occurred via monolayer chemisorption. The adsorption performance of Mo(VI)-MIIP did not significantly decrease, even after six adsorption-desorption cycles, demonstrating that this adsorbent possesses broad application prospects.

ACKNOWLEDGEMENT

This work was financially supported by the National Natural Science Foundation of China (Grant Number 22078157).

CONFLICT OF INTEREST

The authors have no conflict of interests.

DATA AVAILABILITY STATEMENT

All relevant data are included in the paper or its Supplementary Information.

REFERENCES

Adauto, A., Khan, S., Augusto Da Silva, M., Gomes Neto, J. A., Picasso, G. & Sotomayor, M. D. P. T. 2020 Synthesis, characterization and application of a novel ion hybrid imprinted polymer to adsorb Cd(II) in different samples. *Environmental Research* **187**, 109669.

Akbarnejad, S., Amooey, A. A. & Ghasemi, S. 2019 High effective adsorption of acid fuchsin dye using magnetic biodegradable polymer-based nanocomposite from aqueous solutions. *Microchemical Journal* **149**, 103966.

Akhond, M., Pashangeh, K., Karbalaei-Heidari, H. R. & Absalan, G. 2016 Efficient immobilization of porcine pancreatic α-amylase on amino-functionalized magnetite nanoparticles: characterization and stability evaluation of the immobilized enzyme. *Applied Biochemistry and Biotechnology* **180** (5), 954–968.

Al Abri, A. M., Mohamad, S., Abdul Halim, S. N. & Abu Bakar, N. K. 2019 Development of magnetic porous coordination polymer adsorbent for the removal and preconcentration of Pb(II) from environmental water samples. *Environmental Science and Pollution Research* **26** (11), 11410–11426.

Ardau, C., Frau, F., Dore, E. & Lattanzi, P. 2012 Molybdate sorption by Zn-Al sulphate layered double hydroxides. *Applied Clay Science* **65–66**, 128–133.

Ardestani, F., Hosseini, M. H., Taghizadeh, M., Pourjavid, M. R. & Rezaee, M. 2016 Synthesis and characterization of nanopore Mo(VI)-imprinted polymer and its application as solid phase for extraction, separation and preconcentration of molybdenum ions from water samples. *Journal of the Brazilian Chemical Society* **27** (7), 1279–1289.

Atia, A. A. 2008 Adsorption of chromate and molybdate by cetylpyridinium bentonite. *Applied Clay Science* **41** (1), 73–84.

Azizi, N., Abbasi, F. & Abdoli-Senejani, M. 2017 Thiamine immobilized on silane-functionalized magnetic nanoparticles for catalytic synthesis of 2,3-dihydroquinazolin-4(1H)-ones in water. *Materials Chemistry and Physics* **196**, 118–125.

Bukowska, A., Bukowski, W., Hus, K., Depciuch, J. & Parlinska-Wojtan, M. 2017 Synthesis and characterization of new functionalized polymer-Fe_3O_4 nanocomposite particles. *Express Polymer Letters* **11** (1), 2–13.

Dahaghin, Z., Mousavi, H. Z. & Boutorabi, L. 2017a Application of magnetic ion-imprinted polymer as a new environmentally-friendly nonocomposite for a selective adsorption of the trace level of Cu(II) from aqueous solution and different samples. *Journal of Molecular Liquids* **243**, 380–386.

Dahaghin, Z., Mousavi, H. Z. & Sajjadi, S. M. 2017b A novel magnetic ion imprinted polymer as a selective magnetic solid phase for separation of trace lead(II) ions from agricultural products, and optimization using a Box–Behnken design. *Food Chemistry* **237**, 275–281.

Du, J., Li, J., Yang, L. & Lu, J. 2003 Sensitive and selective determination of molybdenum by flow injection chemiluminescence method combined with controlled potential electrolysis technique. *Analytica Chimica Acta* **481** (2), 239–244.

Elwakeel, K. Z., Shahat, A., Khan, Z. A., Alshitari, W. & Guibal, E. 2020 Magnetic metal oxide-organic framework material for ultrasonic-assisted sorption of titan yellow and rose bengal from aqueous solutions. *Chemical Engineering Journal* **392**, 123635.

Fallah, N., Taghizadeh, M. & Hassanpour, S. 2018 Selective adsorption of Mo(VI) ions from aqueous solution using a surface-grafted Mo(VI) ion imprinted polymer. *Polymer* **144**, 80–91.

Fayazi, M., Taher, M. A., Afzali, D., Mostafavi, A. & Ghanei-Motlagh, M. 2016 Synthesis and application of novel ion-imprinted polymer coated magnetic multi-walled carbon nanotubes for selective solid phase extraction of lead(II) ions. *Materials Science and Engineering: C* **60**, 365–373.

Gao, B., Li, X., Chen, T. & Fang, L. 2014 Preparation of molybdate anion surface-imprinted material for selective removal of molybdate anion from water medium. *Industrial & Engineering Chemistry Research* **53** (11), 4469–4479.

Hassan, S. S. M., Kamel, H., A, A., Hassan, A., Amr, A. E. E., Abd El-Naby, H., Al-Omar, M. A. & Sayed, A. Y. A. 2020 $CuFe_2O_4$/polyaniline (PANI) nanocomposite for the hazard mercuric ion removal: synthesis, characterization, and adsorption properties study. *Molecules* **25** (12), 2721.

Hassanpour, S. & Taghizadeh, M. 2016 Rapid and selective separation of molybdenum ions using a novel magnetic Mo(VI) ion imprinted polymer: a study of the adsorption properties. *RSC Advances* **6** (102), 100248–100261.

Hassanpour, S., Taghizadeh, M. & Yamini, Y. 2018 Magnetic Cr(VI) ion imprinted polymer for the fast selective adsorption of Cr(VI) from aqueous solution. *Journal of Polymers and the Environment* **26** (1), 101–115.

He, J., Shang, H., Zhang, X. & Sun, X. 2018 Synthesis and application of ion imprinting polymer coated magnetic multi-walled carbon nanotubes for selective adsorption of nickel ion. *Applied Surface Science* **428**, 110–117.

He, F., Lu, Z., Song, M., Liu, X., Tang, H., Huo, P., Fan, W., Dong, H., Wu, X. & Xing, G. 2019 Construction of ion imprinted layer modified $ZnFe_2O_4$ for selective Cr(VI) reduction with simultaneous organic pollutants degradation based on different reaction channels. *Applied Surface Science* **483**, 453–462.

Kong, D., Zhang, F., Wang, K., Ren, Z. & Zhang, W. 2014 Fast removal of Cr(VI) from aqueous solution using Cr(VI)-imprinted polymer particles. *Industrial & Engineering Chemistry Research* **53** (11), 4434–4441.

Kumar, A., Balouch, A., Abdullah & Pathan, A. A. 2019 Synthesis, adsorption and analytical applicability of Ni-imprinted polymer for selective adsorption of Ni^{2+} ions from the aqueous environment. *Polymer Testing* **77**, 105871.

Li, L., Chen, L., Zhang, H., Yang, Y., Liu, X. & Chen, Y. 2016 Temperature and magnetism bi-responsive molecularly imprinted polymers: preparation, adsorption mechanism and properties as drug delivery system for sustained release of 5-fluorouracil. *Materials Science and Engineering: C* **61**, 158–168.

Li, M., Meng, X., Liang, X., Yuan, J., Hu, X., Wu, Z. & Yuan, X. 2018 A novel In(III) ion-imprinted polymer (IIP) for selective extraction of In(III) ions from aqueous solutions. *Hydrometallurgy* **176**, 243–252.

Liang, Q., Geng, J., Luo, H., Fang, W. & Yin, Y. 2017 Fast and selective removal of Cr(VI) from aqueous solutions by a novel magnetic Cr(VI) ion-imprinted polymer. *Journal of Molecular Liquids* **248**, 767–774.

Lou, Z., Wang, J., Jin, X., Wan, L., Wang, Y., Chen, H., Shan, W. & Xiong, Y. 2015 Brown algae based new sorption material for

fractional recovery of molybdenum and rhenium from wastewater. *Chemical Engineering Journal* **273**, 231–239.

Mercante, L. A., Andre, R. S., Schneider, R., Mattoso, L. H. C. & Correa, D. S. 2020 Free-standing SiO_2/TiO_2–MoS_2 composite nanofibrous membranes as nanoadsorbents for efficient Pb(II) removal. *New Journal of Chemistry* **44** (30), 13030–13035.

Najafi, E., Aboufazeli, F., Lotfi Zadeh Zhad, H. R., Sadeghi, O. & Amani, V. 2013 A novel magnetic ion imprinted nano-polymer for selective separation and determination of low levels of mercury(II) ions in fish samples. *Food Chemistry* **141** (4), 4040–4045.

Nchoe, O. B., Klink, M. J., Mtunzi, F. M. & Pakade, V. E. 2020 Synthesis, characterization, and application of β-cyclodextrin-based ion-imprinted polymer for selective sequestration of Cr(VI) ions from aqueous media: kinetics and isotherm studies. *Journal of Molecular Liquids* **298**, 111991.

Peng, J., Wang, X., Jiang, C., Wang, M., Ma, Y. & Xiang, X. 2014 Separation of Mo(VI) and Fe(III) from the acid leaching solution of carbonaceous Ni-Mo ore by ion exchange. *Hydrometallurgy* **142**, 116–120.

Qi, X., Gao, S., Ding, G. & Tang, A. 2017 Synthesis of surface Cr(VI)-imprinted magnetic nanoparticles for selective dispersive solid-phase extraction and determination of Cr(VI) in water samples. *Talanta* **162**, 345–353.

Ren, Y., Liu, P., Feng, J., Ma, J., Wen, Q. & Zhang, M. 2013 Selective recognition of molybdenum(VI) from water by Mo(VI) oxy ion-imprinted particle as an adsorbent. *Chemical Engineering Journal* **219**, 286–294.

René, W., Lenoble, V., Chioukh, M. & Branger, C. 2020 A turn-on fluorescent ion-imprinted polymer for selective and reliable optosensing of lead in real water samples. *Sensors and Actuators B: Chemical* **319**, 128252.

Shafizadeh, F., Taghizadeh, M. & Hassanpour, S. 2019 Preparation of a novel magnetic Pd(II) ion-imprinted polymer for the fast and selective adsorption of palladium ions from aqueous solutions. *Environmental Science and Pollution Research* **26** (18), 18493–18508.

Tanjim, M., Rahman, M. A., Rahman, M. M., Minami, H., Hoque, S. M., Sharafat, M. K., Gafur, M. A. & Ahmad, H. 2018 Mesoporous magnetic silica particles modified with stimuli-responsive P(NIPAM-DMA) valve for controlled loading and release of biologically active molecules. *Soft Matter* **14** (26), 5469–5479. [PubMed: 29923579].

Tsoi, Y., Ho, Y. & Leung, K. S. 2012 Selective recognition of arsenic by tailoring ion-imprinted polymer for ICP-MS quantification. *Talanta* **89**, 162–168.

Wang, X., Shen, Z., Sang, T., Cheng, X., Li, M., Chen, L. & Wang, Z. 2010 Preparation of spherical silica particles by Stöber process with high concentration of tetra-ethyl-orthosilicate. *Journal of Colloid and Interface Science* **341** (1), 23–29.

Wang, R., Wu, P., Cui, Y., Fizir, M., Shi, J. & He, H. 2020 Selective recognition and enrichment of sterigmatocystin in wheat by thermo-responsive imprinted polymer based on magnetic halloysite nanotubes. *Journal of Chromatography A* **1619**, 460952.

Xiong, Y., Wang, H., Lou, Z., Shan, W., Xing, Z., Deng, G., Wu, D., Fang, D. & Biswas, B. K. 2011 Selective adsorption of molybdenum(VI) from Mo-Re bearing effluent by chemically modified astringent persimmon. *Journal of Hazardous Materials* **186** (2), 1855–1861.

Xiong, Y., Song, Y., Tong, Q., Zhang, P., Wang, Y., Lou, Z., Zhang, F. & Shan, W. 2017 Adsorption-controlled preparation of anionic imprinted amino-functionalization chitosan for recognizing rhenium(VII). *Separation and Purification Technology* **177**, 142–151.

Yang, Z., Zhang, L., Zhang, Y., Bai, M., Zhang, Y., Yue, Z. & Duan, E. 2020 Effects of apparent activation energy in pyrolytic carbonization on the synthesis of MOFs-carbon involving thermal analysis kinetics and decomposition mechanism. *Chemical Engineering Journal* **395**, 124980.

Zeng, J., Dong, Z., Zhang, Z. & Liu, Y. 2017 Preparation of a surface-grafted imprinted ceramic membrane for selective separation of molybdate anion from water solutions. *Journal of Hazardous Materials* **333**, 128–136.

Zhang, L., Xue, J., Zhou, X., Fei, X., Wang, Y., Zhou, Y., Zhong, L. & Han, X. 2014 Adsorption of molybdate on molybdate-imprinted chitosan/triethanolamine gel beads. *Carbohydrate Polymers* **114**, 514–520.

Zheng, H. & Yoshikawa, M. 2015 Molecularly imprinted cellulose membranes for pervaporation separation of xylene isomers. *Journal of Membrane Science* **478**, 148–154.

Zhou, Z., Liu, X., Zhang, M., Jiao, J., Zhang, H., Du, J., Zhang, B. & Ren, Z. 2020 Preparation of highly efficient ion-imprinted polymers with Fe_3O_4 nanoparticles as carrier for removal of Cr(VI) from aqueous solution. *Science of The Total Environment* **699**, 134334.

First received 22 September 2020; accepted in revised form 30 November 2020. Available online 14 December 2020